nature cell biology

Amoeboid T lymphocytes require the septin cytoskeleton for cortical integrity and persistent motility

Aaron J. Tooley[1,4], Julia Gilden[1,4], Jordan Jacobelli[1], Peter Beemiller[1], William S. Trimble[2], Makoto Kinoshita[3] and Matthew F. Krummel[1,5]

The systems that refine actomyosin forces during motility remain poorly understood. Septins assemble on the T-cell cortex and are enriched at the mid-zone in filaments. *Septin* knockdown causes membrane blebbing, excess leading-edge protrusions and lengthening of the trailing-edge uropod. The associated loss of rigidity permits motility, but cells become uncoordinated and poorly persistent. This also relieves a previously unrecognized restriction to migration through small pores. Pharmacologically rigidifying cells counteracts this effect, and relieving cytoskeletal rigidity synergizes with septin depletion. These data suggest that septins tune actomyosin forces during motility and probably regulate lymphocyte trafficking in confined tissues.

An important feature of T lymphocytes is their migration through tissues in search of antigen presenting cells (APC) bearing peptide–MHC complexes. Both motility rate and access to tissues by T cells are highly controlled — this is thought to be necessary to prevent accumulation in peripheral tissues and the potential breakdown of tolerance mechanisms. Motile T cells are characterized by an amoeboid 'hand-mirror' shape in which the trailing edge pinches distinctly into a uropod. This morphology is required for efficient migration within lymph nodes and peripheral tissues, for crossing barriers to enter new tissues and for their reactivity to antigen-bearing APC[1]. Their migration is characterized by actin polymerization at the leading-edge 'pseudopod'[2–4] and myosin IIA-based contraction, predominantly away from the leading edge[5]. Some of the polarity circuits restricting leading-edge extensions to the pseudopods and retraction to the uropod may be similar to those in neutrophils[6] and *Dictyostelium*[7]. The mechanisms that fine-tune protrusive activity and regulate the shape of the uropod, however, remain undetermined.

Septins were first identified as cell division cycle (cdc) mutants[8] in yeast *Saccharomyces cervisiase* and assemble into concentric filaments at the mother-bud neck during cell division[9,10]. The septin ring around the cytokinetic furrow in *S. cerevisiae* functions as a diffusion barrier, maintaining cell-fate determinants in the appropriate cell[11,12]. Individual septins were independently identified in mammals on the basis of their abnormal expression in a wide range of tumours, including mammary adenocarcinomas[13] and myeloid leukaemias[14]. Additionally, the septin 9 locus is a site of frequent retroviral insertion, leading to generation of T-cell lymphomas[15]. Since their identification in mammals, septins have been shown to be important in many cell types, including neurons, platelets and spermatozoa[16–18].

Septins are cytoskeletal proteins that polymerize to form rings and gauzes[19], and typically attach to the cell membrane through amino-terminal phosphoinositide-binding motifs. In mammals, they frequently colocalize with actin stress fibres. The mammalian septins can be divided into four groups. Filaments form from combinations of these, with members of each class potentially substituting for one another and generating a great diversity of possible arrays. A recently reported crystal structure of complexed septins indicates that the essential subunit of septin superstructures is a linear hexamer of septin 2–septin 6–septin 7 with a 2:2:2 stoichiometry[20].

Here we demonstrate a crucial role for septins in T-cell motility. Septins assemble along the cell cortex, enriched in an array of fibrous strands in the mid-zone. Elimination of the septin cytoskeleton using short hairpin RNA (shRNA) led to marked elongation of the uropod, pronounced blebbing and excess leading-edge protrusions, indicative of uncontrolled cytoskeletal forces. Although myosin II activity is required for these phenotypes, there is no evidence that either actin or myosin is overactive in these cells. Rather, the motion and membrane dynamics of septin-deficient cells is consistent with a loss of membrane tension. The resulting disorganized migration of septin-deficient cells strongly suggests a corset-like function for the septin cytoskeleton, providing compression and rigidity, and supporting efficient motion of motile T cells.

RESULTS

Septin filaments assemble on the cortex, enriched in the T-cell mid-zone

We first identified expression of septin 9 by T cells in a gene-trap screen[21] for molecules that polarized in T cells (data not shown).

[1]The Department of Pathology, University of California, San Francisco, 513 Parnassus Avenue, San Francisco, CA 94143-0511, USA. [2]Program in Cell Biology, Hospital for Sick Children and Department of Biochemistry, University of Toronto, 555 University Avenue, Toronto, M5G 1X8, Canada. [3]Biochemistry and Cell Biology Unit, HMRO, Kyoto University Graduate School of Medicine, Yoshida Konoe, Sakyo, Kyoto 606-8501, Japan.
[4]These authors contributed equally to this work.
[5]Correspondence should be addressed to M.F.K. (e-mail: matthew.krummel@ucsf.edu)

Received 9 June 2008; accepted 16 September 2008; published online 30 November 2008; DOI: 10.1038/ncb1808

© 2008 Macmillan Publishers Limited. All rights reserved.

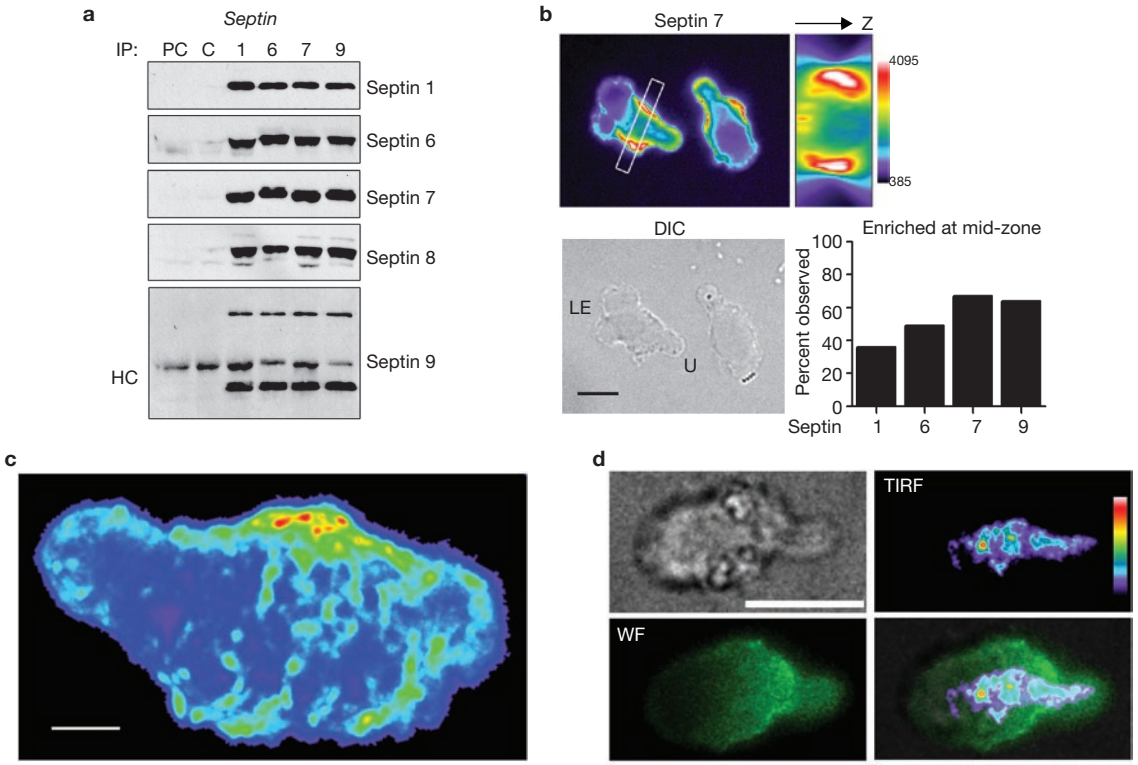

Figure 1 Septin complexes form in T cells, assemble on the cortex and form filaments and puncta in the mid-zone. (**a**) Septins form heteromeric complexes in D10 T cells. Septins 1, 6, 7 or 9 were immunoprecipitated from D10 lysate and blotted for expressed septins. Normal rabbit serum was used to pre-clear (PC) the lysate and as a control for the immunoprecipitation (C). The band present in all samples in the septin 9 blot corresponds to the heavy chain (HC) of the antibody used for the immunoprecipitation. (**b**) Septins localize to the cell cortex in crawling D10 T cells and are frequently enriched in the mid-zone. Crawling D10 T cells were fixed and stained for septins 1, 6, 7 and 9 (septin 7 shown; anti-septin 8 antibodies did not reproducibly stain fixed cells) and the portion of samples with significant enrichment at the mid-zone was quantified by blind-scoring septin 7 ($n = 67$), septin 9 ($n = 64$), septin 1 ($n = 66$) and septin 6 ($n = 68$). Results shown are pooled totals from three independent experiments. A three-dimensional reconstruction of a transverse section (indicated by the white box), demonstrating the presence of an annular septin 7 collar at the T-cell mid-zone (LE, leading edge; U, uropod). (**c**) Confocal images of anti-septin 7 staining were acquired, and a maximum-intensity projection was compiled. Distinct punctate and fibrous regions of septin 7 are found in the T-cell mid-zone and uropod, indicating the presence of septin filaments. All are at or near the cortex (two others are shown in Supplementary Information, Movie 1). (**d**) Composite TIRF and wide-field (WF) imaging also demonstrates that fibrous septin 7 is at or near the coverslip surface. Cells were stained with anti-septin 7 and illuminated by TIRF (shown as pseudocolor) or wide-field (shown as green) illumination. Scale bars, 3 μm (**c**) and 10 μm (**b**, **d**).

Analysis of *septin* expression in a murine T-cell line (Supplementary Information, Fig. S1a) by RT–PCR indicated expression of multiple *septins*, comprising one from Group I (*septin 9*), three from Group II (*septins 6, 8, 11*), two from Group III (*septins 2, 4*) and one from Group IV (*septin 7*). This RNA expression pattern is consistent with expression profiling of human septins[22]. Using a panel of anti-septin-specific polyclonal antibodies, we also detected septin 1 and septins 6–9 protein. We did not have suitable reagents to assess septin 10 expression, and other septins were not present above our level of detection (Supplementary Information, Fig. S1b and data not shown). As septins are known to form heteromeric complexes[23–26], we looked for septin complexes in lysates from D10 T cells. Immunoprecipitation of septins 1, 6, 7 or 9 caused co-precipitation of complexes containing the majority of septins 1, 6, 7, 8 and 9 (Fig. 1a; Supplementary Information, Fig. S5a). Although this method does not reveal the diversity of filament compositions, individual septins were clearly involved in interactions with aggregates containing every other septin.

Four anti-septin antibodies proved suitable for wide-field immunofluorescence microscopy. These grossly highlighted the cell cortex in crawling T cells and were frequently enriched through the mid-zone, forming an annular septin 'corset'. This pattern was most prevalent for septins 7 and 9 and less so for septins 1 and 6 (Fig. 1b). More rarely, and only for septin 9, we observed staining inside the cell near the microtubule-organizing centre (MTOC; data not shown). Similar distributions were observed in primary cells (Supplementary Information, Fig. S2e).

Higher resolution confocal imaging revealed that the mid-zone distribution was highlighted by denser arrays and fibres that were partially perpendicular to the axis of travel (Fig. 1c; Supplementary Information, Movie 1). These septin densities are similar to the stays of a corset or sail: latitudinally-oriented features in an otherwise uniform band. Total internal reflection fluorescence microscopy (TIRF) indicated that regions of adhesion also contained these fibrous arrays (Fig. 1d). Fibres are near the limits of optical resolution (≤250 nm) in width and vary from short puncta to filaments longer than 3 μm. These enrichments are not simply areas of higher membrane density, as septin staining did not colocalize with membrane dyes such as DiO (Supplementary Information, Fig. S2a). In some cells, particularly for septin 6, distributions were predominantly punctate (Supplementary Information, Fig. S2b). These may represent shorter fibres, loosely connected septin structures, subcortical vesicles or another sub-region of the greater septin array. Septin

© 2008 Macmillan Publishers Limited. All rights reserved.

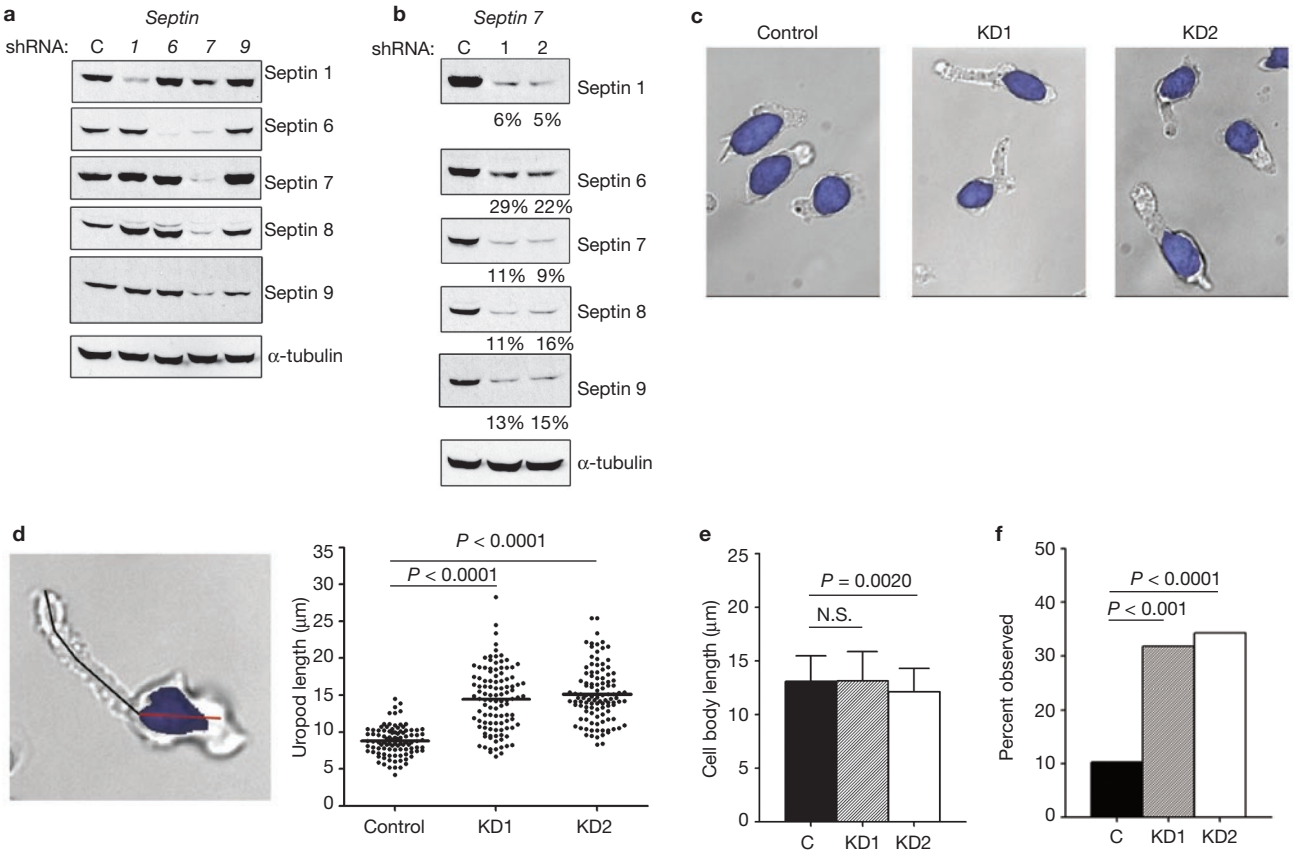

Figure 2 *Septin* knockdown in T cells results in augmented length and bending of uropods. (**a**) Individual shRNAs against *septins 1*, *6*, *7*, *9* and a negative-control shRNA (C) were transfected into D10 T cells. Protein levels were examined by western blotting 72 h after transfection. *Septin 7*^{KD} results in the loss of all other known septins. For septin 9, only the predominant 40K isoform is shown; however, the larger isoforms were reduced as well (data not shown). This result confirms the specificity of the antibodies used throughout this study. (**b**) Reduction in septin complexes is specific for septin 7. A second shRNA at a distinct location was generated to confirm that the results were specific for targeting septin 7. (**c**) *Septin 7*^{KD} D10 T cells have morphological defects, as shown by an increase in uropod length. Hoechst 33342 was used to distinguish the nucleus (highlighted in blue) from the cytoplasm. (**d**) Increased uropod length in *septin 7*^{KD} T cells A line was drawn from the end of the uropod to the nucleus (black line, left panel). (**e**) Normal cell body length of control and *septin 7*^{KD} T cells, measured as in **d** for cell body region (red line in **d**). (**f**) Bent uropods in the absence of septin complexes. A uropod was scored as bent if a straight line could not be drawn through the cell from the distal tip of the uropod to the beginning of the nucleus. For panels **d**–**f**, data shown are mean ± s.d. (**d**, **e**) or pooled totals (**f**) of three independent experiments (*septin 7*^{KD1}, $n = 107$; *septin 7*^{KD2}, $n = 108$; control shRNA cells, $n = 97$). Statistical analysis was performed using a Kruskal-Wallis test with Dunn's post-test (**d**, **e**) or the χ^2 test (**f**).

puncta were also the dominant distribution in rounded, non-motile T cells (Supplementary Information, Fig. S2d), suggesting a functional relationship of the septin corset to T-cell crawling. Finally, we occasionally observed cells with excess leading-edge protrusions in wild-type T cells, and septins, notably septin 6, were present in these protrusions (Supplementary Information, Fig. S2c). In summary, a cortical array of septins decorates the surface of T lymphocytes.

Global morphological and cortical defects in the absence of septins

To assess the function of septins in T cells, we targeted *septins* 1, 6, 7 and 9 using plasmid-based shRNAs. We achieved significant knockdown of these *septins* in D10 T cells when each was specifically targeted (Fig. 2a; Supplementary Information, Fig. S5b). In addition, targeting of *septin 7* eliminated the entire septin complex (Fig. 2a, b). This result was specific for *septin 7* knockdown (*septin 7*^{KD}), as the reciprocal was not observed when other septins were targeted, supporting the hypothesis that septin 7 is crucial for septin assembly[23–25,27].

To confirm that these results were specific for *septin 7*^{KD}, we generated another shRNA targeting septin 7 (*septin 7*^{KD2}) at a distinct site. Expression of either shRNA resulted in similar reductions in all septins (Fig. 2b). We reproducibly achieved greater than 80% knockdown of *septins 6–9*, and more than 70% of *septin 1* using either *septin 7*^{KD1} or *septin 7*^{KD2}. Although *septin* knockdown causes cell division defects in other systems[26–28], no such defects were seen in *septin 7*^{KD} D10 T cells during the 72 h period in which our observations were made (Supplementary Information, Fig. S3a).

There was no apparent phenotype of individual *septin 1*, *6* or *9* deficiencies, but the *septin 7*^{KD}-induced loss of all septins caused profound disruption in cell morphology and motility. The most obvious morphological disruption was in cell length (Fig. 2c, d). The average uropod length in knockdown cells was 14.4 ± 4.3 μm for *septin 7*^{KD1} (mean ± s.d., $n = 107$) and 15.1 ± 3.7 μm for *septin 7*^{KD2} ($n = 108$), compared with 8.8 ± 2.0 μm for control shRNA-treated cells ($n = 97$). In contrast, cell body length was unchanged in *septin 7*^{KD} cells (Fig. 2e), showing that septins were not globally controlling cell size but were particularly necessary

© 2008 Macmillan Publishers Limited. All rights reserved.

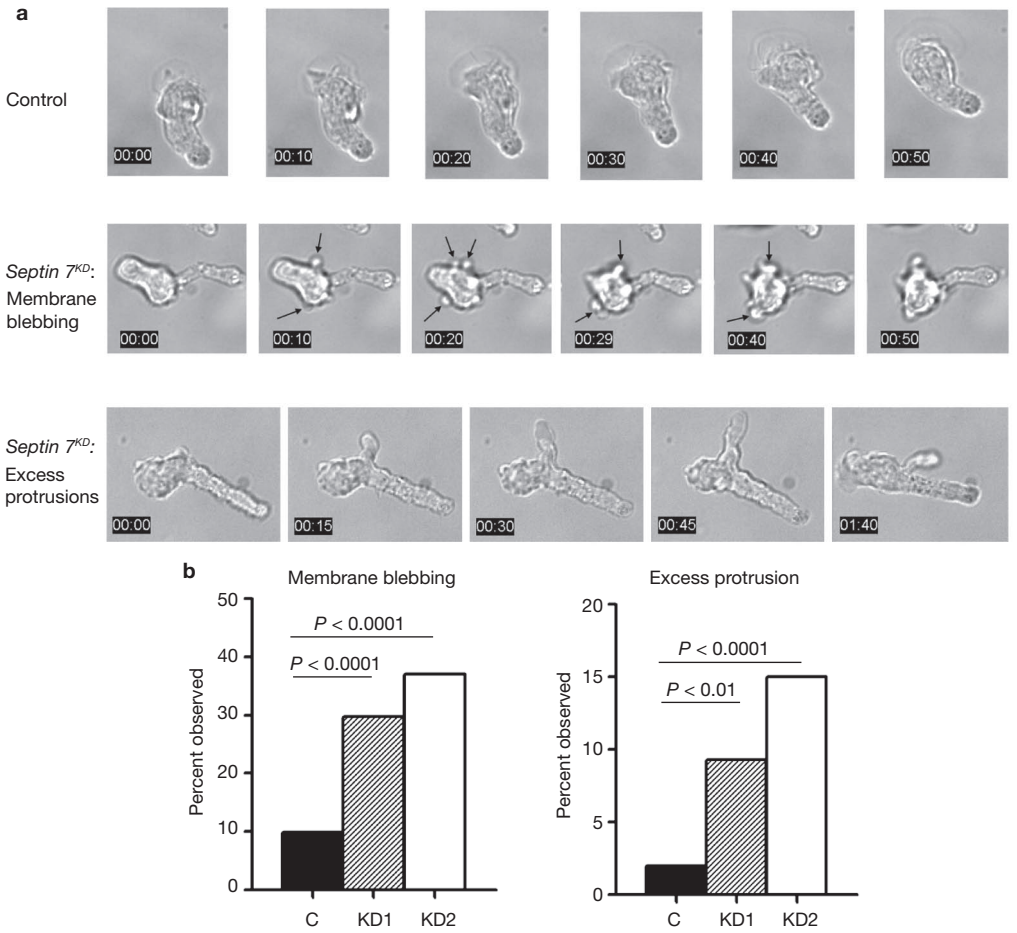

Figure 3 Septin complexes are required for structural stability of the cell cortex and at the T-cell mid-zone. (**a**) *Septin 7*^{KD} T cells have structural defects resulting in membrane blebbing and excess membrane protrusions (also see Supplementary Information, Movies 2–4). Membrane blebbing was dynamic and mainly confined to the cell body. Excess protrusions emanated from both the leading edge and the T-cell mid-zone and persisted as long, thin membrane appendages that were eventually reabsorbed in the mid-zone/rear. Scale bar, 10 μm (**b**). Quantification of structural defects observed in *septin 7*^{KD} T cells. Data shown are pooled totals from three independent experiments. Statistical analysis was performed using the χ^2 test.

to regulate the mid-zone/uropod. The phenotype was independent of adhesion, as cells floating in suspension were also elongated (data not shown).

The long uropods of *septin 7*^{KD} cells also frequently appeared bent (Fig. 2c, d, f). This was observed in 32% of *septin 7*^{KD1} ($n = 107$) and 34% of *septin 7*^{KD2} ($n = 108$) cells, but only 10% of control cells ($n = 97$). This further suggests a stabilizing role for septins in maintaining and coordinating the morphology of motile cells.

Defects due to septin disruption were not confined to the uropod and also suggested poor structural integrity of the cortex. By analysing time-lapse images (Fig. 3a, Supplementary Information, Movies 2–4), we quantified two defects in the leading-edge region: membrane blebbing and excess protrusions, both of which were uncommon in wild-type T cells. Membrane blebbing was dynamic and mainly confined to the cell body (Fig. 3a). Blebbing was observed in 29.7% (*septin 7*^{KD1}, $n = 118$) and 37.1% (*septin 7*^{KD2}, $n = 140$) of *septin 7*^{KD} T cells, compared with 9.9% of the wild-type sample ($n = 151$) (Fig. 3b). Cells frequently blebbed during pauses in motility (Fig. 3a and Supplementary Information, Movie 3), perhaps due to poor coordination of compression and elongation. Although blebbing is often associated with apoptosis, *septin 7*^{KD} and control cells had similar annexin V staining (Supplementary Information, Fig. S3b), suggesting that blebs associated with septin-deficiency arose through another pathway. Time-lapse analysis also demonstrated the formation of long, thin appendages that emanated from both the leading edge and the mid-zone in *septin 7*^{KD} cells before eventually being re-absorbed. Although these protrusions occurred less frequently than membrane blebbing (Fig. 3b), there were significantly more excess protrusions in *septin 7*^{KD} T cells (*septin 7*^{KD1}, 9.3%; *septin 7*^{KD2}, 15.0%) than in the control-treated population (2.0%).

Normal tubulin and actin cytoskeletal activities in the absence of septins

As many of the defects in *septin 7*^{KD} cells resemble those of an overactive cytoskeleton, we analysed the localization and activity of a complement of tubulin and actomyosin-related proteins. Tubulin and pericentrin staining was grossly normal in *septin 7*^{KD} cells, although bundled microtubules were elongated through their uropods (Fig. 4a). Staining for pericentrin revealed normal positioning of the MTOC, directly behind the nucleus (Fig. 4b). These data indicate that the *septin 7*^{KD} phenotype was not due to disorganization of microtubules.

© 2008 Macmillan Publishers Limited. All rights reserved.

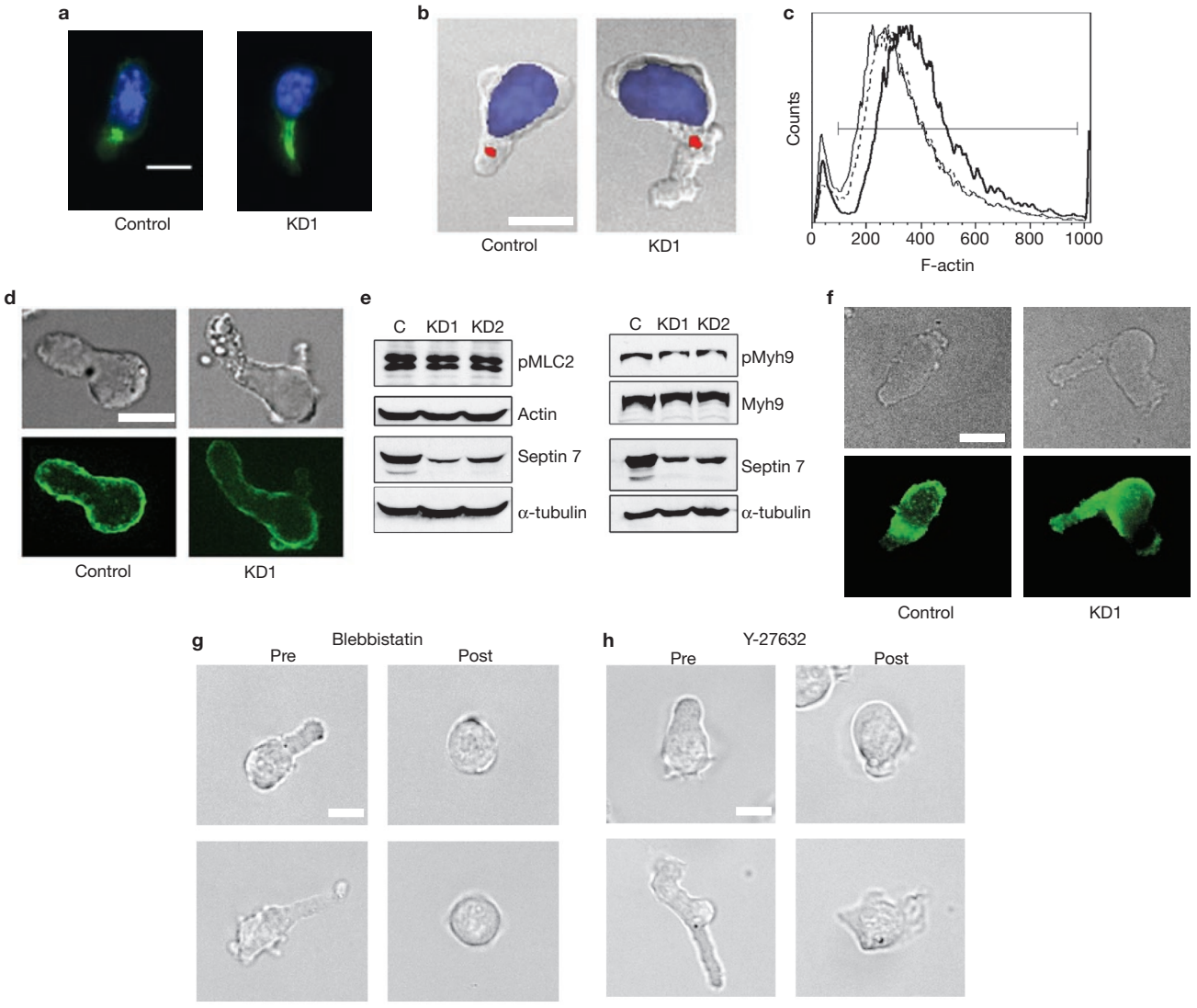

Figure 4 Integrity of tubulin and actomyosin cytoskeletons in septin-deficient T cells. (**a**, **b**)The tubulin cytoskeleton was assessed using DAPI (blue) and anti-tubulin (green, **a**) or anti-pericentrin (red, **b**) antibodies in control and *septin 7*^{KD} cells. The pericentrin-containing MTOC (red) was correctly positioned behind the nucleus (DAPI, blue) in more than 97% of both control and septin-deficient cells with at least 34 cells scored. (**c**) FACS analysis of phalloidin staining. F-actin levels were slightly reduced in septin-deficient cells. (control, bold line; *septin 7*^{KD1}, solid line; *septin 7*^{KD2}, dotted line). Levels of total actin were not altered in these cells (shown in **e**). Similar results were obtained in three independent experiments (**d**) Overall distribution of actin as assessed by immunofluorescence microscopy was cortical for both control and *septin 7*^{KD} cells. (**e**) Myosin II was not overactive in *septin 7*^{KD} T cells. Lysates from control or *septin 7*^{KD} cells were assessed by western blotting for the phosphorylation of the myosin light chain (pMLC2, Ser 19) and heavy chain (pMyh 9). (**f**) Staining for pMLC (Ser 19). Active myosin light-chain kinase was not overabundant in the mid-zone in *septin 7*^{KD} cells. (**g**, **h**) Treatment of cells with the myosin II inhibitor blebbistatin or with the ROCK inhibitor Y-27632 resulted in T-cell rounding and loss of blebs, indicating that these molecules were still required for uropod formation in the absence of septin complexes. T-cell rounding was observed in more than 95% of cells scored for both inhibitors, with at least 84 cells scored from three independent experiments. Results were similar for *septin 7*^{KD2} (data not shown). Scale bars, 10 μm.

Although an overactive actomyosin cytoskeleton could cause the blebbing, elongation and protrusions observed in septin-deficient T cells, we observed a 10–30% reduction in the levels of F-actin in septin-deficient cells, as assessed by phalloidin staining (Fig. 4c), which was not due to changes in the total actin protein level (Fig. 4e; Supplementary Information, Fig. S5c). Phalloidin staining of T cells was grossly normal, with polymerized actin lining the cortex and mildly enriched at the mid-zone in both control and *septin 7*^{KD} cells (Fig. 4d). There were also no detectable differences in the phosphorylation state of myosin light chain (MLC) or myosin heavy chain IIA (Myh9), or changes in the overall levels of myosin II in *septin 7*^{KD} cells (Fig. 4e; Supplementary Information, Fig. S5c). Similarly, in both control and *septin 7*^{KD} cells, phospho-MLC staining was uniformly distributed and mildly enriched in the cell body, relative to the uropod (Fig. 4f). We would have expected additional enrichment of phospho-MLC in the mid-zone/uropod if septins directly regulated MLC activity there. Despite these results, the blebbing, elongation and protrusions of *septin 7*^{KD} cells strongly required myosin II activity. Treatment of *septin 7*^{KD} and control cells with the myosin II inhibitor blebbistatin or a Rho kinase inhibitor Y-27632, essential for MLC activity in the uropod, resulted in complete loss of the uropod and existing blebs (Fig. 4g, h; Supplementary Information, Movies 5, 6).

© 2008 Macmillan Publishers Limited. All rights reserved.

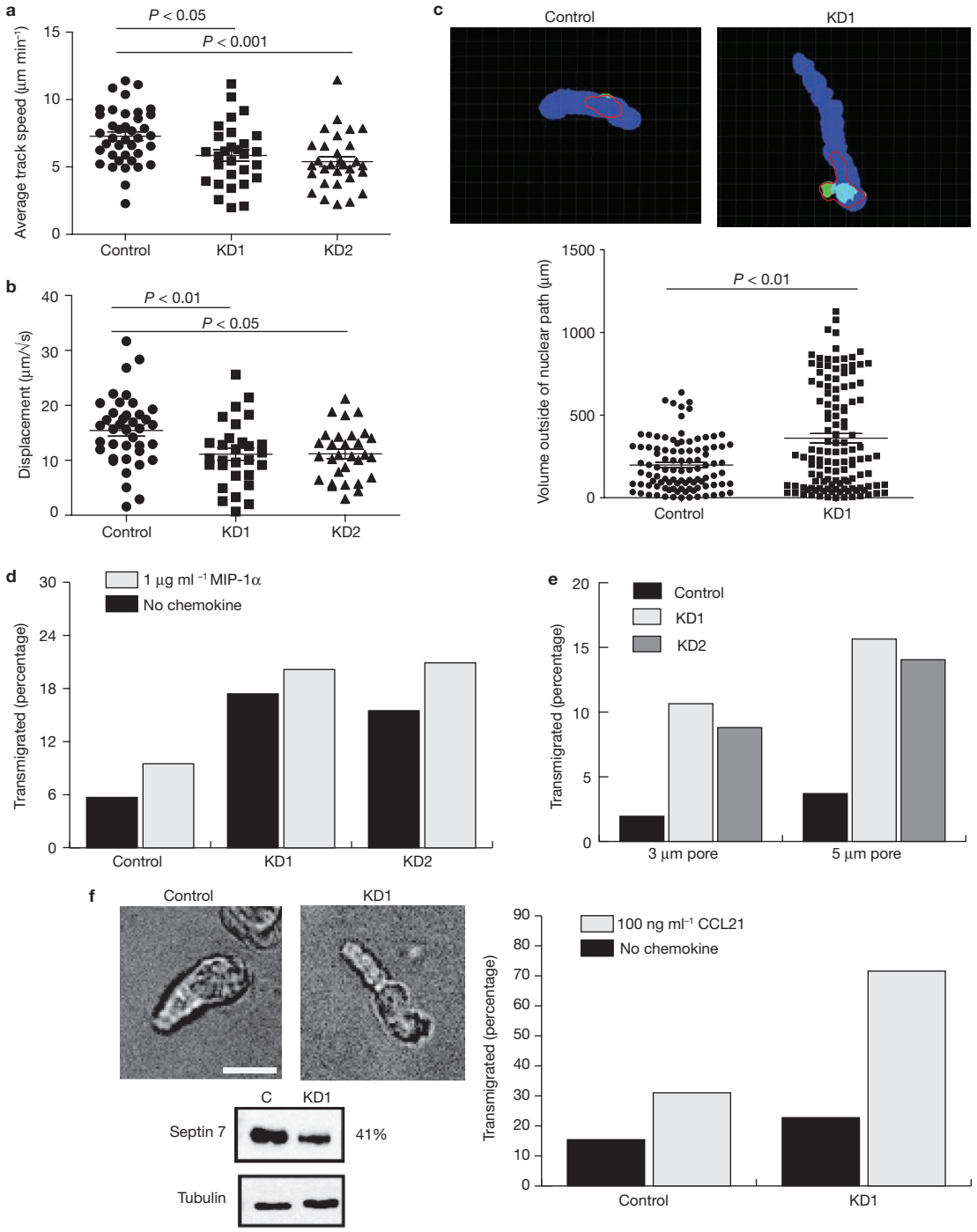

Figure 5 Septins regulate motility and transmigration. (**a**, **b**) Overall crawling velocity (**a**) and displacement (**b**) over time were reduced by *septin 7*^{KD} (*Septin 7*^{KD1}, $n = 31$, *septin 7*^{KD2}, $n = 29$ and control-treated cells $n = 39$). Similar results were obtained in three independent experiments. Statistical analysis was performed using Kruskal-Wallis tests with Dunn's post-tests. (**c**) Top panels show representative frames from analysis of extranuclear path volume. The path of the nucleus over the entire time course is shown in blue. Measured cell body volume deviating from that path is represented in green. The red line shows the outline of the entire cell volume, for reference. The bottom panel shows analysis of multiple time-points for at least 10 different cells and a Mann-Whitney U test indicates that *septin 7*^{KD} cells make significantly more protrusions out of the direction of motility than control cells. (**d**) Responsiveness of control and *septin 7*^{KD} T cells to MIP-1α chemokine gradients in a transwell assay using 8-μm pores. Both control and *septin 7*^{KD} cells had weak migration to the chemokine, but migration of *septin 7*^{KD} cells through the pores was approximately twofold better than control cells. (**e**) *Septin 7*^{KD} T cells transmigrated through extremely small pores, whereas control cells were constrained from passage. Transmigration (in the absence of chemokine) was assessed using transwells with 3-μm and 5-μm pores. Results are representative of three independent experiments. (**f**) *Septin 7*^{KD} DO11.10 T cell blasts show a similar extended uropod phenotype to *septin 7*^{KD} D10 cells. Scale bar, 10 μm. *Septin 7*^{KD} DO11.10 cells transmigrated more efficiently in response to CCL21 than control cells. Transwell inserts with 5-μm pores were used in these assays. Data shown are representative of two experiments (**d**–**f**).

© 2008 Macmillan Publishers Limited. All rights reserved.

Defective motility in the absence of septins

Septin 7^{KD} T cells showed reduced instantaneous crawling velocities *in vitro* (Fig. 5a). *Septin 7*^{KD} T cells crawled at rates of 7.5 ± 1.9 μm min^{-1} (*septin 7*^{KD1}, $n = 36$) and 7.0 ± 1.8 μm min^{-1} (*Septin 7*^{KD2}, $n = 35$), compared with 8.5 ± 2.6 μm min for control cells ($n = 30$). More significantly, they had shorter net displacements than control cells (control: 15.0 ± 6.1 μm/√s, *septin 7*^{KD1}: 10.81 ± 5.8 μm/√s, *septin 7*^{KD2}: 10.85 ± 4.5 μm/√s). This result is surprising with respect to the findings of Fig. 4 and demonstrates that despite functional actomyosin contraction, septin-deficient cells lack normal processivity. These defects were not due to decreased integrin binding by *septin 7*^{KD} cells (Supplementary Information, Fig. S4a) and primary *septin 7*^{KD} T cells showed similar defects under shear flow conditions (Supplementary Information, Fig. S4b). As *septin 7*^{KD} cells were more protrusive overall than control cells, we wondered whether *septin 7*^{KD} cells were making non-productive protrusions outside the direction of motility that impeded their processivity. To address this, we measured the volume of motile cells that extended outside the path of motility and, therefore, did not propel the cell forward. We labelled the nuclei of GFP-transfected cells with Hoechst 33342 and acquired confocal three-dimensional time-lapse images of crawling cells. We then created volumes representing the paths occupied by the nuclei during 15-min movies (Fig. 5c, blue) showing the overall directions of the cells. The GFP volumes were overlaid on the nuclear path volumes at each time-point and the total volumes (Fig. 5c, red outline) and the volumes extending outside the nuclear path were measured (Fig. 5c, green). The total volumes of control and *septin 7*^{KD} cells were similar, but on average, *septin 7*^{KD} cells had about 1.5 times the extranuclear path volume of control cells (median volumes of 167.8 μm^3 and 249.5 μm^3 for control and *septin 7*^{KD}, respectively), supporting the hypothesis that their excess protrusions do not contribute to processive motion and, therefore, contribute to diminshed motility in *septin 7*^{KD} cells.

Enhanced transmigration in the absence of septins

Although specific chemotaxis of D10 cells to MIP-1α is poor, control and *septin 7*^{KD} T cells responded similarly to this chemokine (Fig. 5d). However, *septin 7*^{KD} showed twofold higher transmigration than control cells through 8-μm pores in the absence of the chemokine. As increased motility cannot account for this greater background transmigration (Fig. 5a), we hypothesized that these cells passed through the pores, which are similar in dimension to the girth of the cells, more efficiently than control cells. When we challenged the cells with transwell pores considerably smaller (3 μm and 5 μm) than their smallest dimension, control-treated D10 cells were essentially unable to pass through the small pores (2.0% and 3.7% migration, respectively). However, *septin 7*^{KD} cells migrated through 3 and 5-μm pores approximately fivefold better than control cells (*septin 7*^{KD1}, 10.7% and 15.7% migration, respectively; *septin 7*^{KD2}, 8.8% and 14.1% migration, respectively) and comparably to wild-type cells facing openings that were almost seven times larger (Fig. 5e). This shows that septins restrict chemokine-independent migration and suggests a cell-intrinsic barrier function of the septin cytoskeleton for cells encountering small junctions.

Because D10 T cells show little specific chemotaxis, we expressed a *septin 7* shRNA in primary T cell blasts, which are more suitable to chemotaxis assays. With knockdown, these cells adopted the same extended-uropod phenotype as septin-deficient D10 cells (Fig. 5f.) In a chemotaxis assay using 5 μm pores, we found that septin-deficient primary cells transmigrated at a rate double that of control cells (Fig. 5f). This was accompanied by a small increase in their transmigration in the absence of the chemokine.

Transmigration efficiency is correlated with cortical rigidity

Because of the extreme compression of large cells migrating through small pores, we hypothesized that loss of cortical rigidity in septin-deficient cells allowed them to transmigrate more efficiently. To investigate this possibility, we sought to pharmacologically mimic or counteract the septin-based loss of rigidity. We treated D10 cells with nocodazole to inhibit microtubule polymerization and relax the cell cortex, or with taxol to stabilize microtubules and rigidify the cortex. Interestingly, taxol treatment has previously been shown to increase cell permeation of collagen gels[29]. After nocodazole treatment, both control and *septin 7*^{KD} cells maintained their uropods, but seemed less compact and often generated multiple leading edges (Fig. 6a.) Conversely, when treated with taxol, both groups had few protrusions and most became rounded (Fig. 6a, b)

Time-lapse images of nocodazole-treated cells indicated that they have a similar protrusive phenotype as that of *septin 7*^{KD} cells. Control cells generally made one or two small protrusions in a 10-min period, whereas *septin 7*^{KD} and nocodazole-treated cells frequently made four or five (Fig. 6c), and the persistence of each protrusion was significantly longer for *septin 7*^{KD} and nocodazole-treated than control cells (Fig. 6e). As with *septin 7*^{KD} cells, protrusions in nocodazole-treated cells were uncoupled from the processive motion of the cell. Although protrusions frequently arose at the leading edge, their growth was not restricted to that region and they extended without adhesion in many directions, sometimes reaching so far back before being retracted that the uropod of the cell took on a forked appearance (Fig. 6f). On average, these protrusions did not extended farther from the cell body than the less frequent protrusions in control cells, although occasionally, very long (>15 μm) protrusions arose from *septin 7*^{KD} and nocodazole-treated cells, but not control cells (Fig. 6d). Additionally, the means shown in Fig. 6d may underestimate the true population means for *septin 7*^{KD} and nocodazole-treated cells because the most severely abnormal protrusions often extended out of the imaging plane, excluding them from this analysis.

As the cortical phenotype after nocodazole treatment was similar to that of *septin 7*^{KD} cells, we compared the migration of *septin 7*^{KD} and nocodazole- or taxol-treated D10 cells through 3-μm transwell pores in the absence of chemokine (Fig. 6g). Interestingly, nocodazole-treated control D10 cells transmigrated comparably to untreated *septin 7*^{KD} cells (8.2 ± 0.7% versus 11.8 ± 0.3% and 12.5 ± 1.8% for *septin 7*^{KD1} and *septin 7*^{KD2}, respectively), whereas few (1.9 ± 0.1%) control cells migrated. When *septin 7*^{KD} cells were treated with nocodazole, the effect was greater than additive (35.1 ± 1.9% of *septin 7*^{KD1} and 30.9 ± 7.7% of *septin 7*^{KD2} cells). Conversely, when cells were stiffened with taxol, less than 1.5% passed through the pores, even among *septin 7*^{KD}. These data support the hypothesis that septin depletion relaxes the cell cortex, allowing highly efficient movement through spaces much smaller than the resting cell diameter.

DISCUSSION

Given the many phenotypic abnormalities of septin-deficient cells, septin filaments, being cortically enriched and punctuated by occasional fibres and puncta, may function as a molecular corset. A thin and uniform septin network prevents blebs at the leading edge where actin and

© 2008 Macmillan Publishers Limited. All rights reserved.

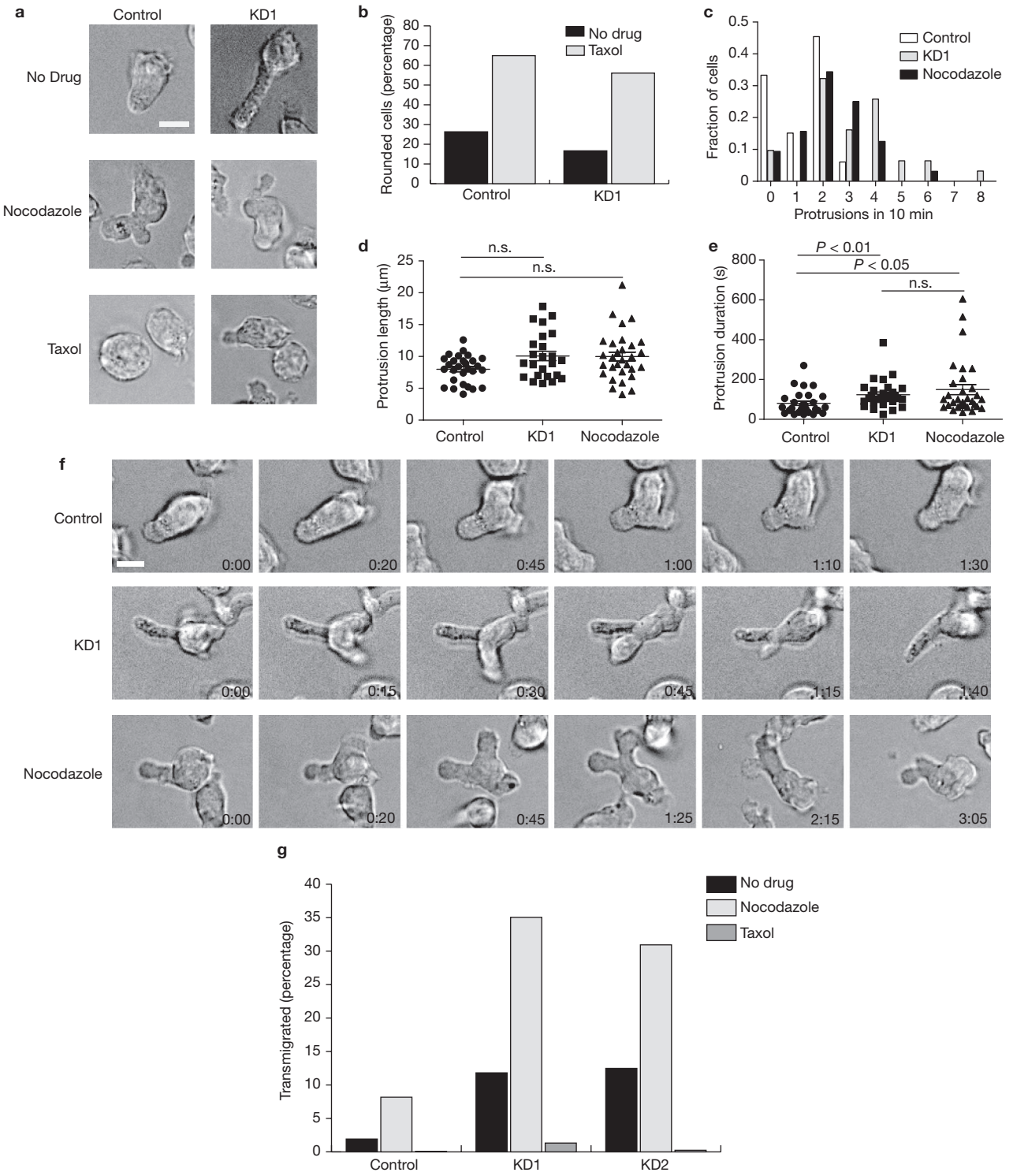

Figure 6 Septins and microtubules regulate rigidity and transmigration. (**a**) Images of control or *septin 7*^{KD} D10 were taken before (no drug) and after treatment with nocodazole (5 μM) or taxol (5 μM) for at least 30 min. (**b**) Taxol treatment caused both *septin 7*^{KD} and control cells to become rounded, suggesting a dependence of the *septin 7*^{KD} phenotype on microtubule function. Data are representative of two independent experiments (control, 52 cells; *septin 7*^{KD}, 35 cells). (**c**) Septin depletion and nocodazole treatment both caused an increase in the number of protrusions made by cells in a 10-min observation period. More than 30 cells per group were analysed. (**d**, **e**) Duration of protrusions (**e**) but not protrusion length (**d**) was significantly increased in both *septin 7*^{KD} and nocodazole-treated cells, compared with control cells. Analysis in **d** and **e** is of the first protrusion observed in each cell from **c**, and was performed using the Kruskal-Wallis test with Dunn's post-test. (**f**) Representative time-lapse images of protrusions observed in control, *septin 7*^{KD} and nocodazole-treated cells. (**g**) Nocodazole caused chemokine-independent transmigration of D10 cells through 3-μm pores similar to and synergizing with that observed in *septin 7*^{KD} cells. This non-specific transmigration was completely abolished by taxol treatment. Cells were treated with drugs for 30 min before the beginning of the 4-h assay. Data shown are representative of two independent experiments. Scale bars, 10 μm.

© 2008 Macmillan Publishers Limited. All rights reserved.

myosin are highly dynamic[30]. We hypothesize that the dynamic turnover of actomyosin filaments and their short length may be complemented by the stays of long septin filaments that are probably stable over time[31,32]. This stability may provide background rigidity against which global and local actomyosin forces are applied.

This fine-tuning of forces is clearly evident in movies of septin-deficient cells; septin loss has a profound effect on coordinated crawling and processivity of D10 cells. We propose that in highly dynamic amoeboid cells, it may be crucial to contain and direct forces generated over their short lengths. At cellular lengths of 5–15 μm, compression forces would tend to propagate across the entire cytoplasm very rapidly[33] and could generate inefficient motility if translated into bulk movements that did not reflect the required directionality. It is therefore interesting to note that foraging *Dictyostelium* lack septins and that their response to chemotactic stimuli, unlike that of T cells, is characterized by increased production of blebs and excess protrusions in multiple directions. Large numbers of protrusions extending in many directions may allow cells to better survey their environments, and *Dictyostelium h*ave evolved to select certain protrusions, rather than restrict their initial number[34].

The cortical instability of septin-deficient cells may be related to their enhanced capacity for migration across small openings. Transwell migration assays assume cells are not able to cross a barrier with dimensions smaller than the resting girth of the cell in the absence of a motive force. We found that this is not the case in the absence of septins. At present, it is unclear whether septin-dependent repression of basal migration is due to additional leading edges (septin-deficient cells find holes more easily) or the loss of cortical stability (septin-deficient cells are more deformable). Although our experiments with nocodazole treatment do not directly distinguish between those possibilities, that cortical stabilization by taxol treatment inhibits transmigration suggests that the relative fluidity of *septin 7*^{KD} cells allows them to pass readily through small pores. As T-cell nuclei are typically larger than 3 μm in diameter, septins may also regulate nuclear shape. Indeed, septins interact with anillin, which, before cell division, is associated with the nuclear envelope[35].

These observations may have important implications for *in vivo* transmigration and tumour metastasis. Cells entering or exiting tissues must squeeze through or between endothelial cells; loss of a basal restriction of this may contribute to metastatic proficiency. As septin expression is frequently altered in human and mouse tumours[22,36,37], and *septin 1* (*Diff6*) was first identified as an overexpressed gene in a tumour line selected for metastasis[38], we speculate that destabilization of the cell cortex due to stoichiometric changes in septin complexes may facilitate tumour metastasis and progression.

METHODS

Cell culture. The D10.G4 CD4+ T cell clone was used in all experiments and was maintained in RPMI 1640 supplemented with 10% fetal calf serum (FCS), L-glutamine, penicillin, streptomycin, β-mercaptoethanol and 50 U ml^{-1} interleukin-2 (IL-2) as described previously[5]. Cells were re-stimulated weekly with conalbumin (134–146) peptide-pulsed irradiated splenocytes from B10.BR donor mice. Primary T cell blasts were generated by stimulating lymph node and spleen cells from DO11.10 TCR transgenic mice *in vitro* with ovalbumin (323–339; 1 μg ml^{-1}) peptide. All mice were bred and maintained in accordance with the guidelines of the Laboratory Animal Resource Center of the University of California at San Francisco.

Antibodies and reagents. The following antibodies were used for cell staining and immunoblotting: anti-phospho-MLC2 (Ser 19) mouse monoclonal no. 3675 (Cell Signaling); anti-actin, clone C4 (Chemicon); anti-α-tubulin clone B-5-1-2 (Sigma); anti-pThr 1939-Myh9, a rabbit polyclonal made against a c-terminal phosphopeptide of Myh9 (ref. 5); rabbit anti-class II myosin polyclonal (BTI); and rabbit polyclonal anti-pericentrin (Covance). Polyclonal anti-peptide antibodies were generated against anti-septin 6C (C)AGGSQTLKRDKEKKN, anti-septin 7 (C) EQQNSSRTLEKNKKKGKIF, anti-septin 8 (C)+ALHATSQQPLRKDKDKKN, and anti-septin 9 (C)IHFEAYRVKRLNEG OR (C)SAMANGVEEKEPEAPEM — two sera generated similar staining and blotting results, where the additional cysteine residues, indicated in parentheses, permitted covalent coupling to Imject Maleimide Activated mcKLH (Pierce Biotechnology) for immunization and to Sulfolink beads (Pierce) for affinity purification. Anti-septin 1 antibodies were generated against a His-tagged sequence of mouse septin 1 (NM_017461) comprising the first 366 amino acids (MDKEYV-GEQSDVL) expressed in *Escherichia coli*. Affinity purified antibodies did not cross react with other septins and detected the predicted band(s). For anti-peptide antibodies, these bands were eliminated if the antibody was pre-incubated with the immunization peptide (data not shown). Specificity was also indicated (Fig. 2) in the specific loss of septins 1, 6 and 9 when these were targeted by shRNA. All antibodies were used at a dilution of 1:100 except for anti-pericentrin, which was used at 1:500 and anti-septin 6, which was used at 1:1000.

Lysis, immunoprecipitation and immunoblotting. D10 T cells were lysed in PBS containing 1% Triton X-100 in the presence of a cocktail of protease and phosphatase inhibitors (2 μg ml^{-1} aprotinin, 2 μg ml^{-1} leupeptin, 2 mM PMSF, 10 mM sodium fluoride, 10 mM iodoacetamide and 1 mM sodium orthovanadate). Equal amounts of cell lysates, as determined with the BioRad detergent-compatible protein assay, were then resolved by SDS–PAGE, and immunoblotting analysis was performed using antibodies described above. For immunoprecipitations, both calcium and magnesium chloride (1 μm each) were added to the lysis buffer, and septin complexes were immunoprecipitated from D10 lysates for 3 h at 4 °C using Protein-A sepharose beads. Lysates were pre-cleared with beads coated with normal rabbit serum.

Cell staining. Cells were incubated at 37 °C on superfrost plus slides (VWR International) for at least 1 h before fixing with 1% paraformaldehyde (supplemented with 1 mM calcium and magnesium chloride) at 37 °C for 10 min. Cells were then centrifuged onto the slides at 200*g* for 5 min. Fixed cells were blocked with 2% donkey serum and permeabilized with 0.2% saponin (Sigma) in PBS for 30 min. Cells were incubated with primary antibodies for 60 min, washed, then stained with secondary antibodies for 60 min. After thorough washing, cells were treated with anti-fade reagent (BioRad) and the slides sealed and imaged. For septin staining, only polarized crawling T cells were scored for enrichment at the T-cell mid-zone. All image analyses and measurements were performed using Metamorph software.

Plasmids and transfections. shRNAs were cloned into the pSilencer 2.0 shRNA expression vector using the human U6 promoter (Ambion) following the manufacturer's instructions. Two hairpins were designed against *septin 7* (*septin 7*^{KD1}, 5′-GGATTTGAATTCACTCTTA-3′ and *septin 7*^{KD2}, 5′-GGATCCGTTTGACCAATTT-3′), targeting the open reading frame and the 3′ untranslated region, respectively. Hairpins against *septin 1* (5′-GCCTGCCCTTGCACTTAAA-3′), *septin 6* (5′-GCTTAAGTCTCTGGACCTAGT-3′) and *septin 9* (5′-GCCTAAGCAAAGTGGTGAACA-3′) were also used in this study. A negative-control vector containing an shRNA with only limited sequence homology to any known sequence in the mouse genome (5′-ACTACCGTTGTTATAGGTG-′3) was used a negative control. Control and shRNA-expressing plasmids were introduced into T cells by electroporation (BioRad) and co-transfection of an EGFP-expressing vector, pEGFP-N1 (Clontech), was used as a positive marker for transfection and for cell sorting. For transfection, 25 μg of plasmid DNA in a molar ratio of shRNA expressing plasmid to GFP reporter greater than 7:1 was used to transfect 50 million cells in a 0.5 ml volume. GFP-positive cells were sorted 48–72 h post-transfection using a MoFlo cell sorter (DakoCytomation). Sorted GFP-positive cells were used approximately 72 h post-transfection in all knockdown experiments in this study.

Retroviral infections. *Septin 7*^{KD1} was cloned into pSIREN-Retro-Q-ZsGreen1 (Clontech), which was then used in calcium phosphate transfection of phoenix cells. Virus-containing supernatant from these cells was used on two consecutive days (days 2 and 3 after activation) to spin-infect DO11.10 T cell blasts. Cells were

© 2008 Macmillan Publishers Limited. All rights reserved.

sorted according to their ZsGreen expression on day 4 and rested for 24 h before experiments were performed.

Microscopy. Imaging experiments were performed using a modified ZeissAxiovert 200M microscope with a plan-neofluor ×40 objective (Carl Zeiss). The microscope was fitted with dual excitation and emission filter wheels and a Coolsnap HQ camera (Roper Scientific). Image acquisition and analysis were performed using Metamorph imaging software (Molecular Devices). To examine T-cell motility *in vitro*, imaging was performed in 0.25% low melting-point agarose and time-lapse images were recorded at 5, 10 and 30-s intervals. For velocity measurements, Hoechst 33342 (1 μg ml^{-1}) was added to the imaging chamber to visualize the nucleus and time-lapse images were acquired at 30-s intervals. Migration of the nucleus was then used to track the cell path for velocity measurements. To examine membrane dynamics, time-lapse images were acquired at higher frequencies (5- and 10-s intervals). Only cells that could be observed for at least 5 min were included in analysis. For extranuclear path volume experiments, initial frames were excluded from analysis, as most of the extranuclear volume in those images was due to the trailing uropod.

Data and statistical analysis. Velocity and displacement were analysed in Imaris (BitPlane). Image processing and measurements for extranuclear path volume was performed in Matlab using Image Processing Toolbox functions (The Mathworks). All statistical analyses were performed using Graphpad Prism and individual tests are named in the figure legends.

Inhibitor studies. When cells were treated with the myosin II inhibitor blebbistatin (racemic, 100 μM final) or ROCK inhibitor Y-27632 (10 μM final), 0.1% low melting-point agarose was used, as the drugs did not diffuse well in 0.25% agarose. Nocodazole and taxol (Sigma-Aldrich) were used at 5 μM, and cells were exposed to the drugs for at least 30 min before those assays. DMSO controls did not alter the morphology or crawling of control or shRNA-treated cells.

F-actin quantification. Cells were fixed immediately after removing from 37 °C to maintain cell morphology. T cells were permeabilized and stained using 3 U of Alexa Fluor 647-conjugated phalloidin according to the manufacturer's protocol (Invitrogen). F-Actin staining was quantified using a BD FacsCalibur and data were analysed using FlowJo (TreeStar).

Transmigration assay. Transmigration assays were carried out using transwells (Corning) with 3-μm, 5-μm or 8-μm pores in the absence of chemokine. Transmigration assays were performed at 37 °C for 4 h in the absence of FCS, before cells were collected and counted for a fixed period of time on a BD FACSCalibur flow cytometer. Data were analysed using CellQuest Facs analysis software.

Note: Supplementary Information is available on the Nature Cell Biology website.

ACKNOWLEDGEMENTS

We thank A. Weiss and M.T. McManus for insight and critical discussions, ShuWei Jiang and Cliff McArthur for expert technical assistance with cell sorting and Christine Lin and Ed Shimazu for computer support. We also thank Cynthia Voong for critical reading of the manuscript and members of the Krummel lab for thoughtful discussions. This work was supported by the NIH(R21-AI062899), the Sandler family fund, the National Science Foundation and the Leukemia and Lymphoma Society.

AUTHOR CONTRIBUTIONS

J.G. and A.T. performed all experiments and wrote the manuscript; J.J. and P.B. assisted with the data analysis and planning the experiments; W.S.T. and M.K. contributed reagents and gave conceptual assistance; M.F.K. coordinated the project and assisted with planning the experiments and writing the manuscript. All authors discussed the results and manuscript text.

COMPETING FINANCIAL INTERESTS

The authors declare no competing financial interests.

Published online at http://www.nature.com/naturecellbiology/
Reprints and permissions information is available online at http://npg.nature.com/reprintsandpermissions/

1. Sanchez-Madrid, F. & del Pozo, M. A. Leukocyte polarization in cell migration and immune interactions. *EMBO J.* **18,** 501–511 (1999).
2. Yan, C. *et al.* WAVE2 deficiency reveals distinct roles in embryogenesis and Rac-mediated actin-based motility. *EMBO J.* **22,** 3602–3612 (2003).
3. Snapper, S. B. *et al.* WASP deficiency leads to global defects of directed leukocyte migration in vitro and *in vivo*. *J. Leukoc. Biol.* **77,** 993–998 (2005).
4. Snapper, S. B. *et al.* N-WASP deficiency reveals distinct pathways for cell surface projections and microbial actin-based motility. *Nature Cell Biol.* **3,** 897–904 (2001).
5. Jacobelli, J., Chmura, S. A., Buxton, D. B., Davis, M. M. & Krummel, M. F. A Single class II myosin modulates T cell motility and stopping but not synapse assembly. *Nature Immunol.* **5,** 531–538 (2004).
6. Xu, J. *et al.* Divergent signals and cytoskeletal assemblies regulate self-organizing polarity in neutrophils. *Cell* **114,** 201–14 (2003).
7. Sasaki, A. T. *et al.* G protein-independent Ras/PI3K/F-actin circuit regulates basic cell motility *J. Cell Biol.* **178,** 185–191 (2007).
8. Koshland, D., Kent, J. C. & Hartwell, L. H. Genetic analysis of the mitotic transmission of minichromosomes. *Cell* **40,** 393–403 (1985).
9. Versele, M. & Thorner, J. Some assembly required: yeast septins provide the instruction manual. *Trends Cell Biol.* **15,** 414–424 (2005).
10. Kinoshita, M. Diversity of septin scaffolds. *Curr. Opin. Cell Biol.* **18,** 54–60 (2006).
11. Barral, Y., Mermall, V., Mooseker, M. S. & Snyder, M. Compartmentalization of the cell cortex by septins is required for maintenance of cell polarity in yeast. *Mol. Cell* **5,** 841–851 (2000).
12. Takizawa, P. A., DeRisi, J. L., Wilhelm, J. E. & Vale, R. D. Plasma membrane compartmentalization in yeast by messenger RNA transport and a septin diffusion barrier. *Science* **290,** 341–344 (2000).
13. Montagna, C. *et al.* The Septin 9 (MSF) gene is amplified and overexpressed in mouse mammary gland adenocarcinomas and human breast cancer cell lines. *Cancer Res.* **63,** 2179–2187 (2003).
14. Osaka, M., Rowley, J. D. & Zeleznik-Le, N. J. MSF (MLL septin-like fusion), a fusion partner gene of MLL, in a therapy-related acute myeloid leukemia with a t(11;17)(q23;q25). *Proc. Natl Acad. Sci. USA* **96,** 6428–6433 (1999).
15. Sorensen, A. B. *et al.* Sint1, a common integration site in SL3-3-induced T-cell lymphomas, harbors a putative proto-oncogene with homology to the septin gene family. *J. Virol.* **74,** 2161–2168 (2000).
16. Ihara, M. *et al.* Cortical organization by the septin cytoskeleton is essential for structural and mechanical integrity of mammalian spermatozoa. *Dev. Cell* **8,** 343–352 (2005).
17. Tada, T. *et al.* Role of Septin cytoskeleton in spine morphogenesis and dendrite development in neurons. *Curr. Biol.* **17,** 1752–1758 (2007).
18. Dent, J. *et al.* A prototypic platelet septin and its participation in secretion. *Proc. Natl Acad. Sci. USA* **99,** 3064–3069 (2002).
19. Rodal, A. A., Kozubowski, L., Goode, B. L., Drubin, D. G. & Hartwig, J. H. Actin and septin ultrastructures at the budding yeast cell cortex. *Mol. Biol. Cell* **16,** 372–384 (2005).
20. Sirajuddin, M. *et al.* Structural insight into filament formation by mammalian septins. *Nature* **449,** 311–315 (2007).
21. Tooley, A. J., Jacobelli, J., Moldovan, M. C., Douglas, A. & Krummel, M. F. T cell synapse assembly: proteins, motors and the underlying cell biology. *Semin. Immunol.* **17,** 65–75 (2005).
22. Hall, P. A., Jung, K., Hillan, K. J. & Russell, S. E. Expression profiling the human septin gene family. *J. Pathol.* **206,** 269–278 (2005).
23. Kinoshita, M., Field, C. M., Coughlin, M. L., Straight, A. F. & Mitchison, T. J. Self- and actin-templated assembly of mammalian septins. *Dev. Cell* **3,** 791–802 (2002).
24. Kremer, B. E., Haystead, T. & Macara, I. G. Mammalian septins regulate microtubule stability through interaction with the microtubule-binding protein MAP4. *Mol. Biol. Cell* **16,** 4648–4659 (2005).
25. Nagata, K., Asano, T., Nozawa, Y. & Inagaki, M. Biochemical and cell biological analyses of a mammalian septin complex, Sept7/9b/11. *J. Biol. Chem.* **279,** 55895–55904 (2004).
26. Surka, M. C., Tsang, C. W. & Trimble, W. S. The mammalian septin MSF localizes with microtubules and is required for completion of cytokinesis. *Mol. Biol. Cell* **13,** 3532–3545 (2002).
27. Spiliotis, E. T., Kinoshita, M. & Nelson, W. J. A mitotic septin scaffold required for Mammalian chromosome congression and segregation. *Science* **307,** 1781–1785 (2005).
28. Nagata, K. *et al.* Filament formation of MSF-A, a mammalian septin, in human mammary epithelial cells depends on interactions with microtubules. *J. Biol. Chem.* **278,** 18538–18543 (2003).
29. Ratner, S., Sherrod, W. S. & Lichlyter, D. Microtubule retraction into the uropod and its role in T cell polarization and motility. *J. Immunol.* **159,** 1063–1067 (1997).
30. Ponti, A., Machacek, M., Gupton, S. L., Waterman-Storer, C. M. & Danuser, G. Two distinct actin networks drive the protrusion of migrating cells. *Science* **305,** 1782–1786 (2004).
31. Caviston, J. P., Longtine, M., Pringle, J. R. & Bi, E. The role of Cdc42p GTPase-activating proteins in assembly of the septin ring in yeast. *Mol. Biol. Cell* **14,** 4051–4066 (2003).
32. Dobbelaere, J., Gentry, M. S., Hallberg, R. L. & Barral, Y. Phosphorylation-dependent regulation of septin dynamics during the cell cycle. *Dev. Cell* **4,** 345–357 (2003).
33. Charras, G. T., Yarrow, J. C., Horton, M. A., Mahadevan, L. & Mitchison, T. J. Non-equilibration of hydrostatic pressure in blebbing cells. *Nature* **435,** 365–369 (2005).
34. Andrew, N. & Insall, R. H. Chemotaxis in shallow gradients is mediated independently of PtdIns 3-kinase by biased choices between random protrusions. *Nature Cell Biol.* **9,** 193–200 (2007).
35. Field, C. M., Coughlin, M., Doberstein, S., Marty, T. & Sullivan, W. Characterization of anillin mutants reveals essential roles in septin localization and plasma membrane integrity. *Development* **132,** 2849–2860 (2005).
36. Russell, S. E. & Hall, P. A. Do septins have a role in cancer? *Br. J. Cancer* **93,** 499–503 (2005).
37. Hall, P. A. & Russell, S. E. The pathobiology of the septin gene family. *J. Pathol.* **204,** 489–505 (2004).
38. Nottenburg, C., Gallatin, W. M. & St John, T. Lymphocyte HEV adhesion variants differ in the expression of multiple gene sequences. *Gene* **95,** 279–284 (1990).

© 2008 Macmillan Publishers Limited. All rights reserved.

nature cell biology

DOI: 10.1038/ncb1808

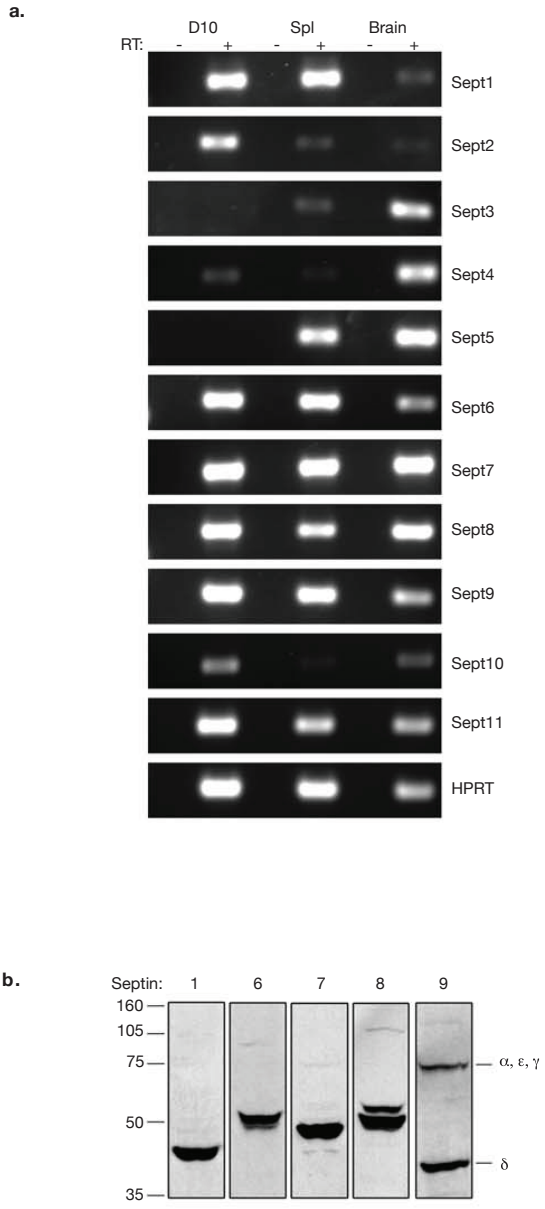

Figure S1 Septin RNA and protein expression in murine T cells. **(a)** RNA was isolated from D10 T cells and whole cell extracts from mouse spleen and brain for positive controls. Septin expression was screened using reverse-transcriptase PCR (RT). Primers used for septin screening are shown in Supplemental Table 1. Primers for Hypoxanthine-guanine phosphoribosyltransferase (5' – CTCGAAGTGTTGGATACAGGC – 3' and 5' – GATAAGCGACAATCTACCAGAG – 3') were used as a positive control to confirm cDNA synthesis was successful. Transcripts for all septins tested except Septins 3 and 5 were present in D10 T cells. Screening primers were designed based on sequence information obtained from the Ensembl database (Supplemental Table 1). Regions common to all known transcripts of individual septins were chosen in order to amplify any possible isoforms expressed in T cells. When multiple transcripts were present, sequences were compared against transcripts found in the GenBank database. Partial mRNA sequence for Septin 12 is present in GenBank (gi:21312733). However, primers designed against that sequence did not amplify a fragment in any of the samples tested. A murine homolog of Septin 13 could not be found via sequence analysis. A putative gene with significant homology to other murine septins was found on chromosome 5 (Ensembl gene ID: ENSMUSG00000034219); however, the expression of this gene was not tested in these samples.(**b**) D10 T cells express Septins 1, 6, 7, 8 and 9. A panel of anti-septin specific polyclonal antibodies was used to screen lysate from D10 T cells in order to determine the septins that were expressed at the protein level. D10 T cells expressed at least two isoforms of Sept8 and Sept9.

© 2008 Macmillan Publishers Limited. All rights reserved.

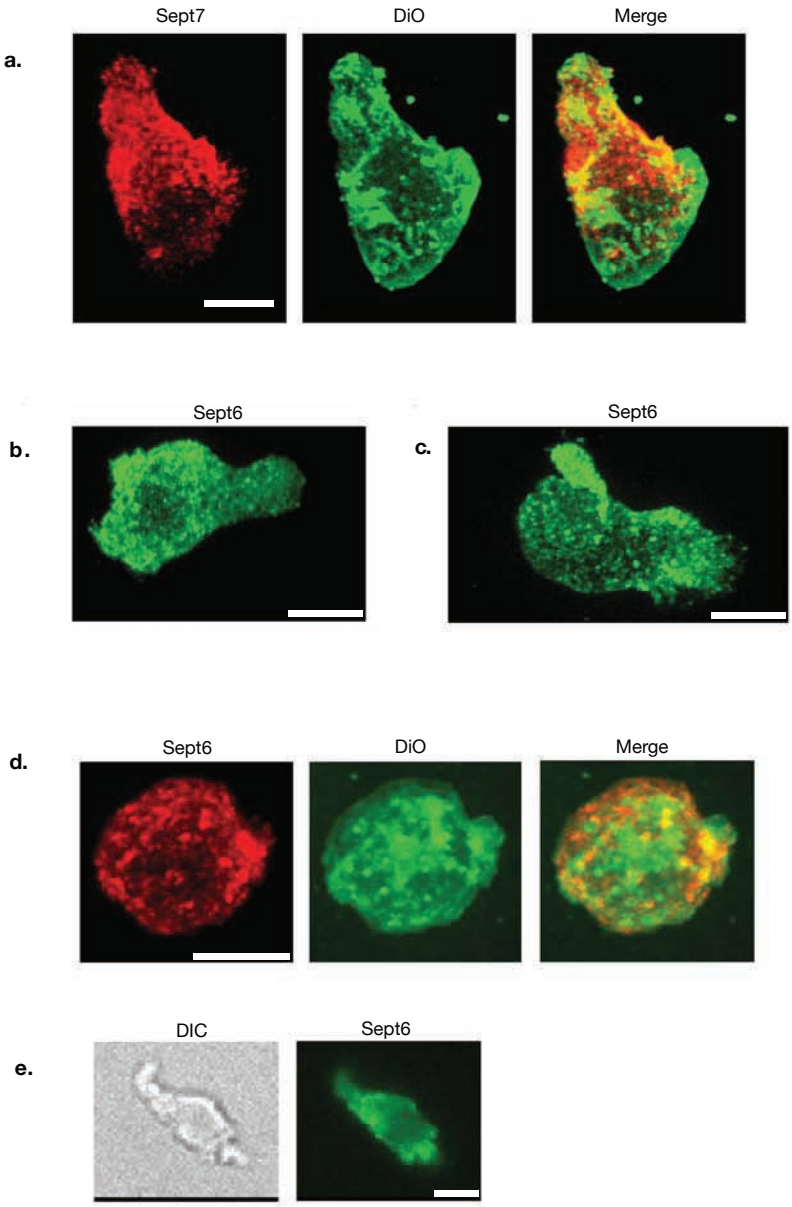

Figure S2 Septin staining is not associated with membrane density and is variably strand-like. (**a**) D10 T cells were stained with anti-Sept7 and the membrane intercalating dye DiO. Poor colocalization indicates that Septin staining was not a result of local variations in membrane densities. (**b**) D10 T cells were stained with anti-Sept6 antibodies. Staining had less fibrous and more punctuate distributions. (**c**) A rare cell with an extra leading edge protrusion shows enrichment of Sept6 in the protrusion. (**d**) A round, nonmotile cell stained for Sept6 demonstrates a punctate, but evenly distributed distribution across the cell cortex. (**e**) A motile primary T cell stained for Sept6 shows a similar cortical staining to that of D10 cells. Scale bars represent 10 μm.

© 2008 Macmillan Publishers Limited. All rights reserved.

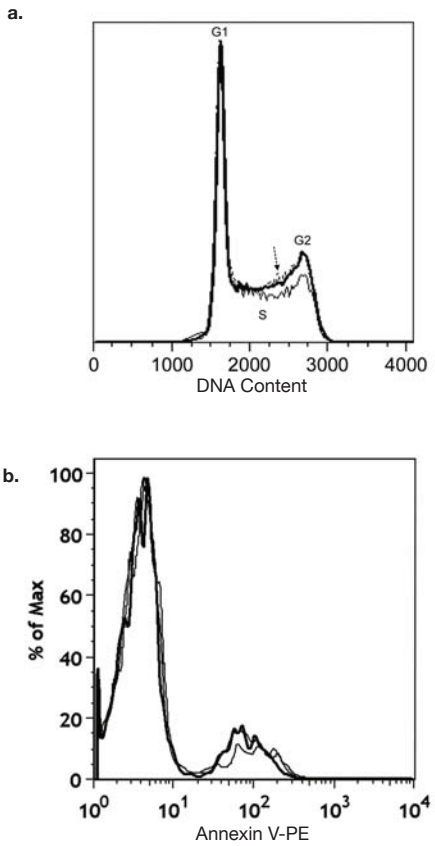

Figure S3 Sept7 knock-down (KD) D10 T cells are not defective in cell division or survival.(**a**) DNA content was examined in Sept7KD and control treated T cells 72 hours post-transfection to determine if Sept7KD T cells had any defects in cell division. Cells were incubated with 10 μg/ml Hoechst 33342 for 45-90 minutes at 37°C and analyzed on a BD LSR II flow cytometer equipped with a UV laser. Profiles of DNA content of Sept7KD T cells, KD #1 (solid line) and KD #2 (dashed line, indicated by arrow) were almost identical to control treated cells (bold line), indicating D10 T cells divide normally in the absence of septin complexes. (**b**) Sorted control (bold line) and Sept7KD cells (solid and dotted lines) were stained for Annexin V-PE (BD) according to the manufacturer's instructions.

© 2008 Macmillan Publishers Limited. All rights reserved.

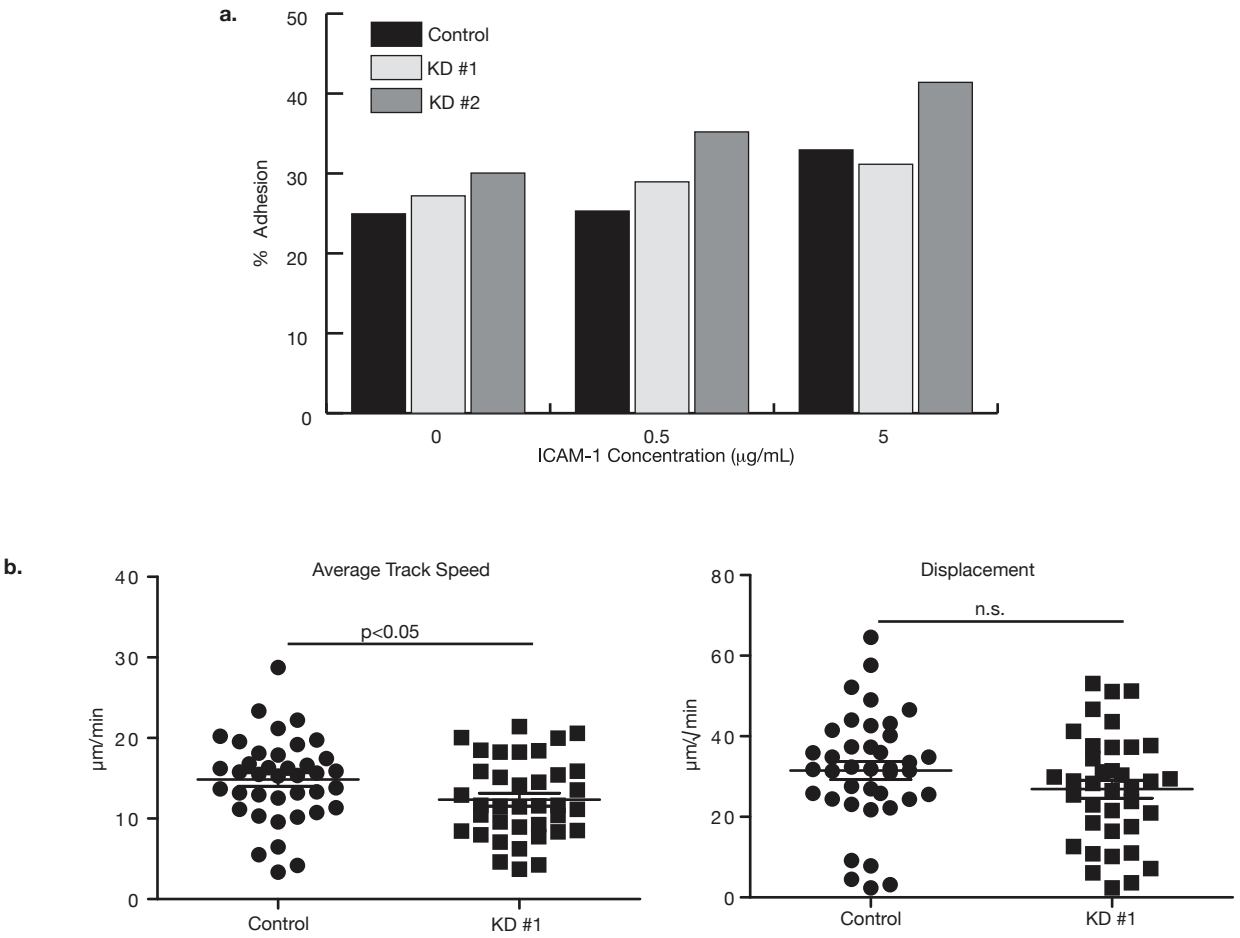

Figure S4 Sept7KD T cells are not defective in integrin-adhesion but demonstrate inefficient motility under laminar flow. (**a**) Control and Sept7KD cells adhere equivalently to ICAM-1. Cells were plated on ICAM-1 coated plastic and allowed to adhere for 1 hour, washed gently, then removed with EDTA and counted by flow cytometry. (**b**) Activated control or Sept7KD DO11 T cells we allowed to adhere on ICAM-coated glass coverslips for 3 minutes and then subjected to shear flow of 1 dyne/cm^3 for 15 minutes while images were collected. Similar to non-flow conditions, Sept7KD cells traveled slower than control cells, though the small difference in their displacements over time did not achieve statistical significance. Data was pooled from two independent experiments and was analyzed with a Mann-Whitney U-test.

© 2008 Macmillan Publishers Limited. All rights reserved.

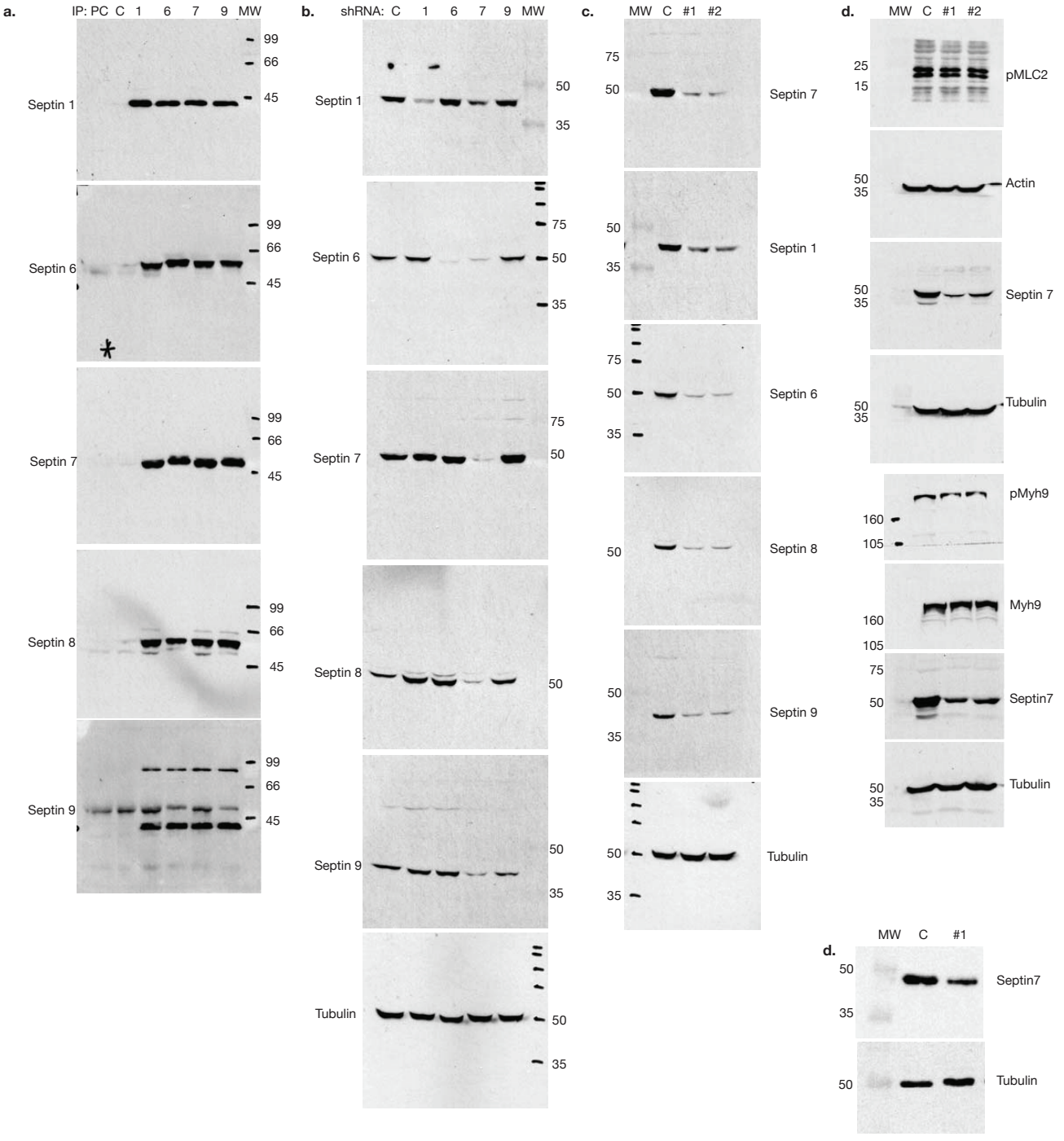

Figure S5 Full-size gel blots demonstrate specificity of antibodies. Full images of gel blots used for analysis in Figures 1a, 2a, 2b, 4e, and 5f (**a, b,** and **c**, respectively.) Images vary in size because many membranes were cut for blotting of multiple proteins.

© 2008 Macmillan Publishers Limited. All rights reserved.

Supplementary Table 1 Primer pairs used for Septin RT-PCR analysis shown in Supplemental Figure S1.

Mouse Septin Gene/Protein	Ensembl Gene ID/ Transcript ID	Chromosome	PCR Primers	Primer Location	Fragment Size (mRNA))
SEPT1/SEPT1	ENSMUSG00000000486 ENSMUST00000000497	Chr. 7	For: 5' - GTATCAAGGTGAAGTTGACCTTGGTGG - 3' Rev: 5' - TCCTCATCAGAGTCACACTCTGGG - 3'	Exon 3 Exon 8	388 bp
SEPT2/SEPT2	ENSMUSG00000026276 ENSMUST00000027495	Chr. 1	For: 5' - TTCGACTGTTGAGATTGAAGAGCGG - 3' Rev: 5' - TTCAATCAACTGGTTGGAGCCAACC - 3'	Exon 5 Exon 9	493 bp
SEPT3/SEPT3	ENSMUSG00000022456 ENSMUST00000077804	Chr. 15	For: 5' - AAGTCAACACTGGTCAACACCCTC - 3' Rev: 5' - TGACAGGAATGATGTTCACCACTTTGC - 3'	Exon 2 Exon 5	397 bp
SEPT4/SEPT4	ENSMUSG00000020486 ENSMUST00000018544	Chr. 11	For: 5' - AAGGAGTATGTGGGCTTTGCAACC - 3' Rev: 5' - TGTTGTTGACTGCATCCCCAAATCC - 3'	Exon 3 Exon 5	292 bp
SEPT5/SEPT5	ENSMUSG00000072214 ENSMUST00000096987	Chr. 16	For: 5' - TGAAACACACCGTCGACATTGAGG - 3' Rev: 5' - TGGAAACTGGTACACGTGGATCC - 3'	Exon 5 Exon 8	398 bp
SEPT6/SEPT6	ENSMUSG00000050379 ENSMUST00000060474	Chr. X	For: 5' -CAGCTGGTGAATAAGTCAGTCAGCC - 3' Rev: 5' - TGATCTTGAACTTTGCCAGCTCACTC - 3'	Exon 2 Exon 5	508 bp
SEPT7/SEPT7	ENSMUSG00000001833 ENSMUST00000060080	Chr. 9	For: 5' - TCCAGGATTTGGAGATGCAGTGG - 3' Rev: 5' - CAAGGATACTGCCTTCCTCTGACTC - 3'	Exon 5 Exon 9	465 bp
SEPT8/SEPT8	ENSMUSG00000018398 ENSMUST00000018542	Chr. 11	For: 5' - TATCTGCAGGAGGAGTTGAAGATCCG - 3' Rev: 5' - GCTTAGGAACTCCTTCCTCTTTGCC - 3'	Exon 4 Exon 8	615 bp
SEPT9/SEPT9	ENSMUSG00000059248 ENSMUST00000019038	Chr. 11	For: 5' - AGACGATCGAAATCAAGTCGATCACC - 3' Rev: 5' - TCCTCATCAAACTCCTTCTGCGG - 3'	Exon 4 Exon 8	430 bp
SEPT10/SEPT10	ENSMUSG00000019917 ENSMUST00000089092	Chr. 10	For: 5' - AGGAAGAACTGAAGATCAAGCGTGC - 3' Rev: 5' - TAGTGCCTCATATGTGTCTGCTCCC - 3'	Exon 3 Exon 6	493 bp
SEPT11/SEPT11	ENSMUSG00000058013 ENSMUST00000074733	Chr. 5	For: 5' - ATGACACAAGGATTCACGCCTGC - 3' Rev: 5' - ATACAACTCGTAGTGGCGAGTGTGC - 3'	Exon 4 Exon 7	464 bp

© 2008 Macmillan Publishers Limited. All rights reserved.

Supplemental movie legends

Movie S1 Three-dimensional renderings of annular and cortical septin bundles. D10 T cells, stained with anti-Septin7 and subjected to confocal imaging as in Figure 1d, were rendered using a maximal intensity projection algorithm to generate a three-dimensional reconstruction. Two cells are shown.

Movie S2 Crawling of control treated D10 T cells. In order to examine membrane dynamics in control treated T cells, time-lapse images were acquired at 5–10 sec intervals for at least 10 min. Imaging was performed in 0.25% low-melting point agarose to limit drifting of non-adherent cells.

Movie S3 Membrane blebbing in Sept7KD D10 T cells. In order to examine membrane dynamics in septin deficient T cells, time-lapse images were acquired at 5–10 sec intervals for at least 10 min. Membrane blebbing is indicated by arrows during the movie. Imaging was performed in 0.25% low-melting point agarose.

Movie S4 Excess protrusions in Sept7KD D10 T cells. In order to examine membrane dynamics in septin deficient T cells, time-lapse images were acquired at 5–10 second intervals for at least 10 min. Excess protrusions were observed for two different cells during the movie and are indicated by arrows. Imaging was performed in 0.25% low-melting point agarose.

Movie S5 Myosin II activity was required for cortical and mid-zone defects in Sept7KD D10 T cells. In order to determine if myosin II activity was still required for uropod formation in septin deficient T cells, control and Sept7KD T cells were treated with the myosin II inhibitor Blebbistatin. Time-lapse images were acquired at 30-sec intervals immediately after addition of the drug. Imaging was performed in 0.10% low-melting point agarose.

Movie S6 ROCK activity was required for cortical and mid-zone defects in Sept7KD D10 T cells. In order to determine if ROCK activity was still required for uropod formation in septin deficient T cells, control and Sept7KD T cells were treated with the ROCK inhibitor Y-27632. Time-lapse images were acquired at 30-sec intervals with addition of the drug after time-point five. Imaging was performed in 0.10% low-melting point agarose to limit drifting of non-adherent cells.

© 2008 Macmillan Publishers Limited. All rights reserved.